Nonlin. Processes Geophys., 20, 935–944, 2013
www.nonlin-processes-geophys.net/20/935/2013/
doi:10.5194/npg-20-935-2013

Nonlinear Processes in Geophysics
Open Access

Asymmetric tide in Lake Vallunden (Spitsbergen)

A. V. Marchenko[1,2] **and E. G. Morozov**[3]

[1]Svalbard University Center, Longyearbyen, Spitsbergen, Norway
[2]Sustainable Arctic Marine and Coastal Technology (SAMCoT), Centre for Research-Based Innovation (CRI), Norwegian University of Science and Technology, Trondheim, Norway
[3]Shirshov Institute of Oceanology, Russian Academy of Sciences, Moscow, Russia

Correspondence to: E. G. Morozov (egmorozov@mail.ru)

Received: 11 December 2012 – Revised: 8 August 2013 – Accepted: 15 August 2013 – Published: 4 November 2013

Abstract. We observed strongly asymmetric tide in a channel connecting the Van Mijen Fjord and Lake Vallunden in Spitsbergen. The channel is approximately 100 m long, 10 m wide, and 1–2 m deep. Asymmetric tide was also observed in the lake. The form of the semidiurnal tide is described by a combination of only three harmonics (M_2, S_2 and M_4) with different amplitudes and phases. The flood dominant form of the surface elevation in the channel (unlike the ebb dominant tide in the fjord) is formed over a horizontal distance of 50 m over a shallow bottom at the entrance to the channel. The tide in shallow places becomes asymmetric due to nonlinear effects caused by the influence of the bottom and especially by choking of the tidal flow over a sill that is located between the fjord and channel. We think that such a small distance, over which the form of the tide changes, is caused by the small scale of the channel related to the fjord. We suggest a numerical model related to these measurements.

1 Introduction

The phenomenon of asymmetric tide is well known. Tidal asymmetry is usually developed in shallow water. If the duration of decreasing sea level due to the ebb exceeds that of the increasing tide (when flood tidal currents are stronger), the system is referred to as flood dominant or flood asymmetric. If the duration of the decreasing tide is shorter than that of the increasing tide (and consequently, the ebb currents exceed the flood currents), the tide is referred to as ebb dominant (Walton, 2002). Usually, asymmetric tide is developed in channels and inlets (Hoitink et al., 2003; Mirfendersk and Tomlinson, 2008). This phenomenon is analyzed in many papers (Gallagher, 1973; Aubrey and Speer, 1985).

The presence of higher harmonics is an additional mechanism for tidal velocity asymmetry in inlets (Boon and Byrne 1981; Aubrey and Speer, 1985). If two tidal constituents (M_2 and M_4) are developed, we can express the tidal elevation of the surface as

$$h = A_{M2}\cos(\omega_{M2}t) + A_{M4}\cos(\omega_{M4}t - \phi), \quad (1)$$

where A_{M2} is the amplitude of M_2 component of tide; and A_{M4} is the amplitude of M_4 component of tide; ϕ is the amplitude phase difference between M_2 and M_4 constituents of tide.

Boon and Byrne (1981) showed that flood dominance exists if $\pi \le \phi \le 2\pi$, and ebb dominance exists if $0 \le \phi \le \pi$. The greater the ratio A_{M4}/A_{M2}, the greater the flood or ebb dominance. If $\phi = 0$, the crests are sharp and troughs are flat. If $\phi = 2\pi$, the crests are flat and troughs are sharp.

We observed strongly asymmetric tide in a channel connecting the Van Mijen Fjord and Lake Vallunden (and also in Lake Vallunden) in Spitsbergen. The channel that connects Lake Vallunden with the fjord (Littrowneset) is a natural test area for investigating strong asymmetric tides. Tides in fjords were investigated by Stigebrandt (1980) and Farmer and Freeland (1983). The studies in Van Mijen Fjord were conducted by Fer and Widell (2007) and Støylen and Weber (2010). Long-term measurements of tides in Van Mijen Fjord were performed by E. Kvale (Caline, 2009). The amplitudes of different tidal constituents based on his measurements are presented in Table 1. We see from the table that M_2 and S_2 constituents dominate in the tidal motion.

The study region is a place where construction of a new bridge is planned, which will connect the Svea coast of the fjord with the new deposits of coal found on the other side of the fjord. The strong currents in that area are likely to cause

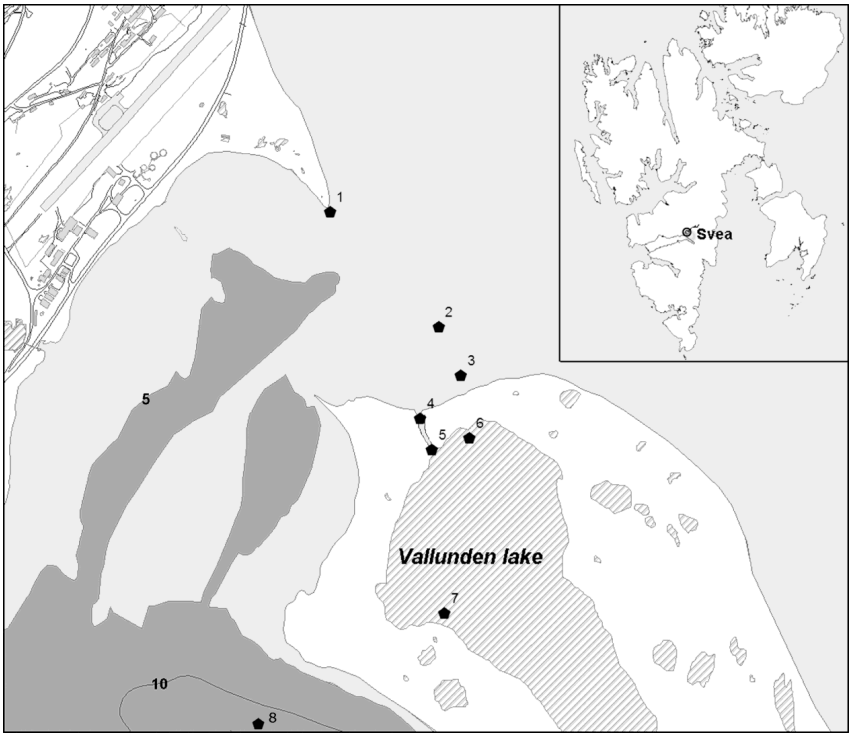

a)

b) c)

Fig. 1. (a) Chart of the region and locations of the instruments. **(b)** Aerial photograph of the lake and channel. **(c)** The channel near the entrance to the lake.

erosion near the bridge pillars. The future causeway and a bridge would reduce the amount of tide water entering the rear part of the fjord, but strong tidal currents between the bridge pillars can occur.

The motivation of this paper is to show that strong tidal asymmetry develops in a small channel that connects the lake with the fjord. The structure of tides becomes flood dominant in the channel and lake. This transition occurs over a small distance of 50 m. Similar effects can develop between the pillars of the bridge.

2 Experiment

Field works were performed in 2008–2012 in Van Mijen Fjord (Spitsbergen). Lake Vallunden, approximately 1 km long, is connected to the Van Mijen Fjord by a shallow channel 100 m long, 10 m wide, and 1–2 m deep (Littrowneset Channel). The lake is located almost near the summit of the fjord at a distance of 80 km from the open ocean. Strong tidal currents develop in this channel because the tidal displacement of the level in the Van Mijen Fjord reaches 3 m. Photos and chart of the region, in which points of measurements are indicated, are shown in Fig. 1.

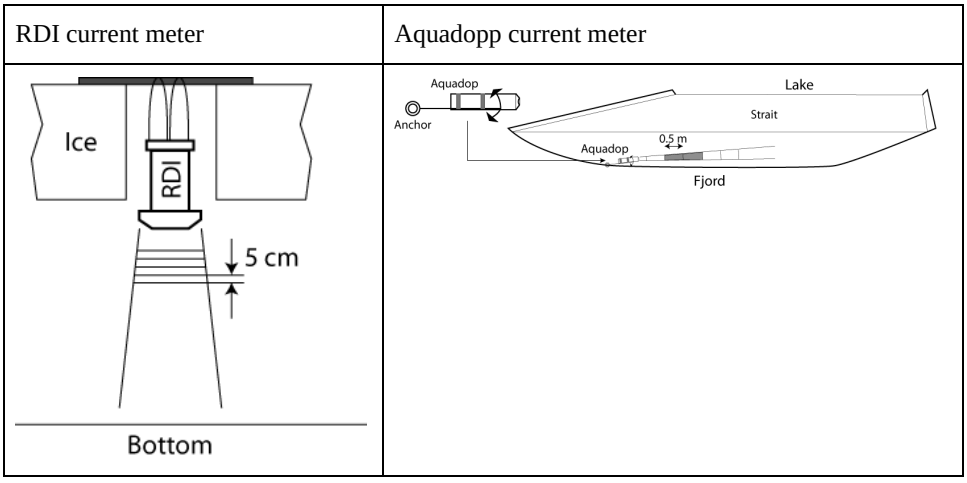

Fig. 2. Deployment schemes of ADCPs: **(a)** RDI Sentinel and **(b)** Aquadopp.

We deployed bottom tide gauges (SBE-26, SBE-39 and SBE-37) in the lake, in the channel, and in the fjord near the channel. We also deployed a current meter (Aquadopp, operating frequency 2 MHz) in the channel and measured the time evolution of the level with graduated poles (vertical pole with marks of centimeters). The currents were measured in the fjord from ice near the channel using an RDI Sentinel instrument (operating frequency 1.2 MHz). A summary of measurements is given in Table 2.

A down-looking acoustic Doppler current profiler (ADCP) RDI Sentinel was deployed in the fjord at point 2 (Fig. 1a) in the wintertime (1.2 MHz, bin size 5 cm, high resolution mode, bottom tracking, time/ping 3.52 min, average ensemble interval 2 min). It was fixed in a hole in the ice as shown in Fig. 2a. The Aquadopp current meter (2 MHz, bin size 50 cm, time sampling 6 s) was located in the channel horizontally as shown in Fig. 2b at point 4 (Fig. 1a). It was tightly fixed at a distance of 20 cm from the bottom of the channel. The second and third bins were averaged so that the instrument measured integrated currents in the interval 0.5–1.5 from the transducer.

3 Data records and analysis

We placed two graduated poles at both ends of the channel (points 4 and 5 in Fig. 1a) and observed the tidal elevation of the level during half of the period of the semidiurnal tide (Fig. 3a). The displacement of the sea level at the fjord side of the channel reached 50 cm at the place where the pole was located in the channel, whereas at the lake side it was only 15 cm. We note that the surface displacement in the fjord reached 1.5 m (Fig. 4). The maximum tide in the lake occurs with a 90 min delay relative to the maximum tide in the fjord. When the currents in the fjord turn from tide to ebb, the current continues to flow into the lake for 90 min. This happens because when the surface elevation starts to decrease in the fjord it is still higher than in the lake, and the equilibrium occurs only after 90 min of the water level decreasing in the fjord (Fig. 3b).

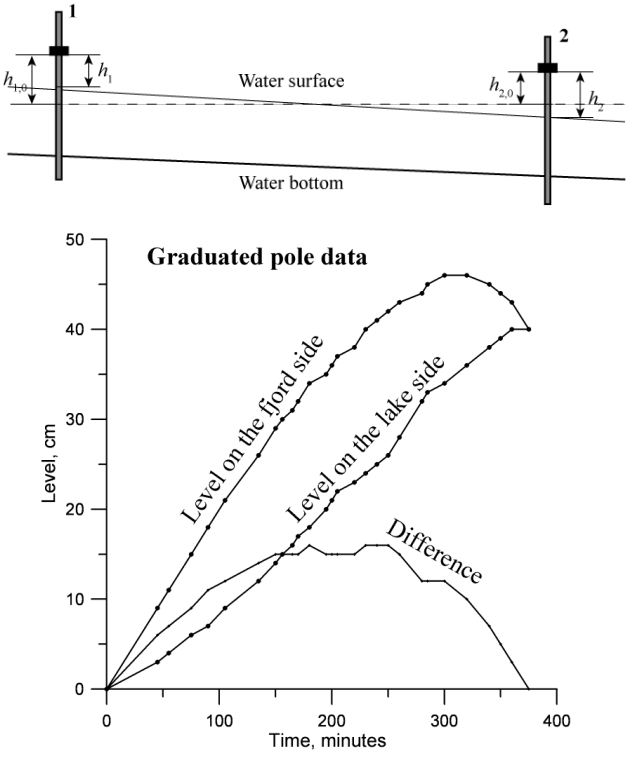

Fig. 3. (a) Scheme of water level measurements using two graduated poles in the channel; **(b)** graphs of sea level variations at two graduated poles in the channel.

In August 2009, two SBE-39 pressure gauges were deployed on the bottom of the lake at points 6 and 7 and

Table 1. Harmonic constants based on the long-term measurements of tide near the Littrowneset Channel.

	M_2	S_2	K_1	K_2	N_2
A, m	0.5109	0.1867	0.0701	0.0541	0.0967
ω, s^{-1}	14.0519×10^{-5}	14.5444×10^{-5}	7.29212×10^{-5}	14.5842×10^{-5}	13.788×10^{-5}
G (phase, grad)	43.51	96.95	238.75	94.84	24.50

Table 2. Summary of measurements.

Time	Points of measurements (see Fig. 1)							
	1	2	3	4	5	6	7	8
September 2008	SBE-39		SBE-39					
August 2009	SBE-26			Graduated pole	Graduated pole	SBE-39	SBE-39	SBE-39
September 2010	SBE-39			ADCP Aquadopp		SBE-39	SBE-39	
February 2009	SBE-39					SBE-39		
March 2012	SBE-37	ADCP RDI				SBE-39		

pressure gauge SBE-26 was deployed on the fjord bottom at point 1 (Fig. 1a). The instruments in the lake recorded clear flood-dominant time series of currents and pressure. The results of measurements are shown in Fig. 4a and c. The tide amplitude in the lake is two times smaller than in the fjord.

The graphs of water pressure in the fjord, on the lake side and on the opposite side of the fjord, based on the data of pressure gauges SBE-39 deployed at points 1 and 3 in September 2008 are shown in Fig. 5. The measurements demonstrate that the amplitude of the tide is almost the same at both shores of the fjord. The records in the channel and in the lake show that the tide record is flood dominant.

The measurements in the lake were repeated in September 2010. In this experiment, one SBE-39 pressure gauge was deployed in the lake at point 6 and a current meter (Aquadopp) was deployed in the channel at point 4. The records of SBE-39 are shown in Fig. 4b and d. The record of currents in the channel at point 4 is shown in Fig. 6. The form of the pressure and current records is flood dominant. The maximum absolute speed of the current in the channel was about $1.5\,m\,s^{-1}$. The measurements were made in the ice-free season using the Aquadopp current meter.

The form of the tide changes because of the presence of a shallow rocky bar where the channel connects with the lake. In summer, the depth of this bar in the low water phase is less than 1 m. In winter the effect of the bar is enhanced by the freezing of ice, which makes the bar even shallower. In winter, strong currents in the channel influence the reduction of ice thickness in comparison with the ice thickness in the fjord and in the lake. At the same time the snow thickness on the ice surface in the channel is greater than in the fjord. Combination of these two effects influences a constriction of the channel. As a result, the tidal amplitude in the lake becomes smaller and the duration of the flood tidal phase in the lake becomes shorter. This effect is shown in Fig. 7. In

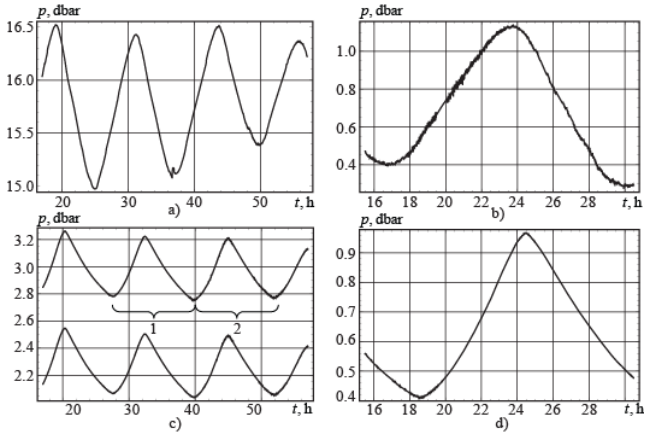

Fig. 4. Seabed water pressure measured in the fjord **(a, b)** and in the lake **(c, d)**. Field works were carried out on 26–28 August 2009 **(a, c)** and 4–5 September 2010 **(b, d)**. Braces with numbers 1 and 2 in **(c)** show the data used to compare with the model calculations.

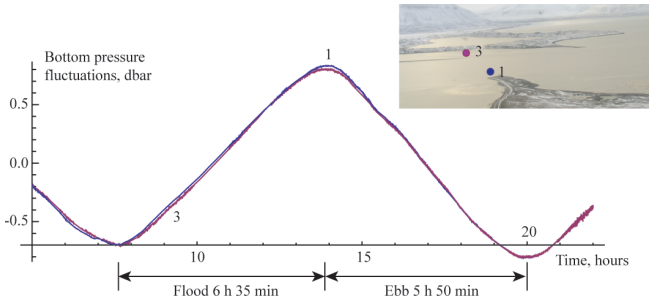

Fig. 5. Bottom pressure variation in the fjord near the channel and on the opposite side of the fjord versus time recorded in September 2008. A photo of the place with red points indicating the locations of measurements is shown in the upper right corner.

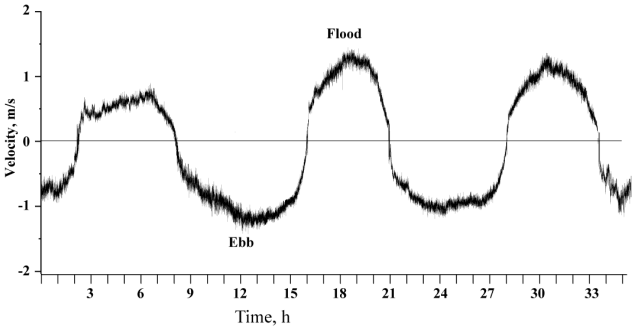

Fig. 6. Record of currents 20 cm over the bottom of the channel (Aquadopp instrument). Measurements were made in September 2010.

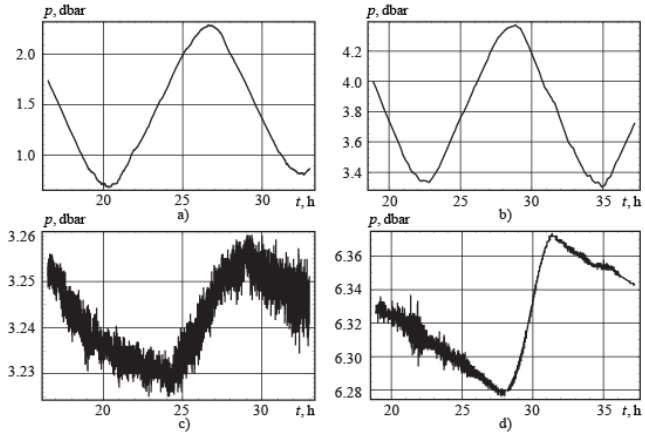

Fig. 7. Seabed water pressure measured in the fjord **(a, b)** and in the lake **(c, d)**. Field works were performed under ice on 8–9 February 2009 **(a, c)** and on 8–9 March 2012 **(b, d)**.

the expeditions in April 2009, 2010, and 2011, the tide in the lake was zero when the channel was completely blocked due to freezing. The measurements of water velocities in the channel during the ice season were not successful because of the strong flood of water on the ice through the drilled holes.

The sea current profile in the fjord was recorded from the ice with ADCP RDI (1.2 MHz) at point 2 on March 2012. The measurements were carried out in a shallow channel in the fjord where the tidal currents are maximal. Examples of the ADCP time series versus time for the velocity direction and velocity magnitude are shown in Fig. 8. The northeastern velocities (60°, blue color) are related to the flood cycle. The flood currents last approximately from 10:00 to 18:20 LT (8 h 20 min). The flood cycle based on the pressure measurements (increasing depth) lasts from 11:30 to 18:05 (6 h 35 min). The southwestern currents (210°, yellow color) are related to the ebb cycle. The ebb currents last approximately from 06:00 to 12:00 LT (6 h) or even shorter because from 09:30 to 12:00 LT; the ebb currents are only in the upper layer, while the lower layer is occupied by the tidal currents. The ebb cycle based on the pressure measurements (decreasing depth) lasts from 05:40 to 11:30 LT (5 h 50 m).

Table 3. Duration of flood and ebb periods at different points in the fjord near the channel.

Points in Fig. 1; date of measurements; figure in which the graph is shown	Duration of periods	
	Flood period	Ebb period
Point 1, September 2008, Fig. 5.	6 h 35 min	5 h 50 min
Point 3, February 2009, Fig. 7a.	6 h 27 min	5 h 57 min
Point 8, August 2009, Fig. 4a.	6 h 49 min	5 h 35 min
Point 1, September 2010, Fig. 4b.	6 h 25 min	5 h 59 min
Point 1, March 2012, Fig. 7b.	6 h 28 min	5 h 56 min
Point 2, March 2012, Fig. 8.	6 h 35 min	5 h 50 min

Table 3 summarizes all measurements in the fjord, near the channel, made in different periods of time.

The maximum absolute velocity of up to 50 cm s^{-1} shown in Fig. 8b (red color) was recorded during a very short time period in the beginning of the ebb phase. Generally, the absolute velocities were lower than 30 cm s^{-1}. The tidal current below the ice in the narrow part of the Van Mijen Fjord between points 1 and 3 is not symmetric over the semidiurnal cycle unlike the water pressure variations at the bottom (Fig. 5). However, the pressure cycle is also asymmetric. Properties of the velocity profile across the fjord depend on the locations were the ice is grounded in the low water phase and on river discharge from the valley at the back of the fjord (Wrangborg et al., 2013).

4 Simulation of bottom pressure variations

We tried to find a fit for the measurements by a bottom pressure gauge at point 6 (see Fig. 1a). A record of the tide gauge in the lake is shown with a blue line with variable amplitude (Fig. 9).

We consider three types of variations.

1. Decreasing or increasing amplitude.
2. Uneven periods of flood and ebb.
3. Sharp crests and flat troughs.

The decreasing amplitude of the tide is related to the spring-neap variability of tides that is caused by the presence of two main semidiurnal tidal constituents M_2 (period 12.42 h) and S_2 (period 12.00 h) (Caline, 2009). In the mathematical sense, this variability is the beating caused by two sinusoids with close frequencies. Irregularity superimposed over this variation is caused by onshore and offshore wind currents that slightly change the regular tidal variation of the level.

Blockage over the bar at the entrance to the channel causes the generation of higher harmonics of the semidiurnal tide (Stigebrandt, 1980; McClimans, 1977); hence the uneven periodicity of flood and ebb tides occurs. Among them the most

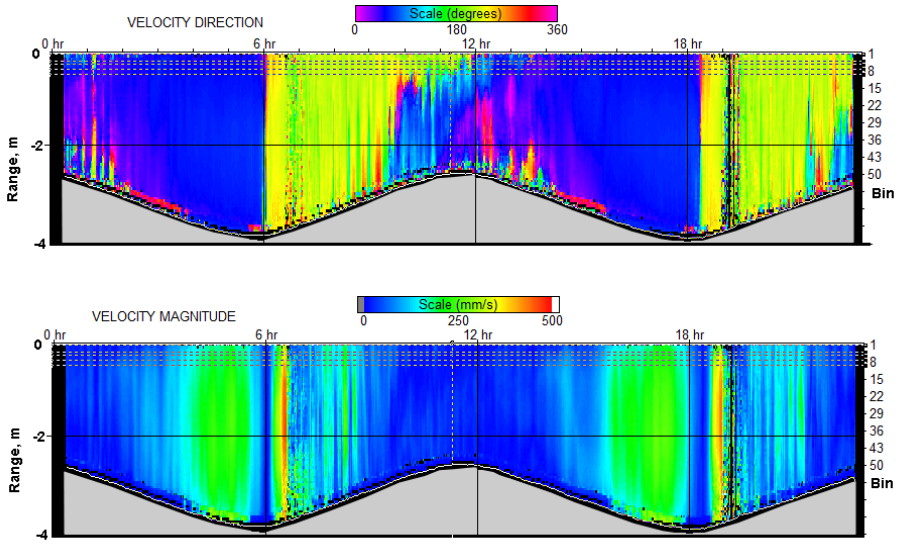

Fig. 8. Record of currents measured by the ADCP instrument at point 2 (see Fig. 1a for its location).

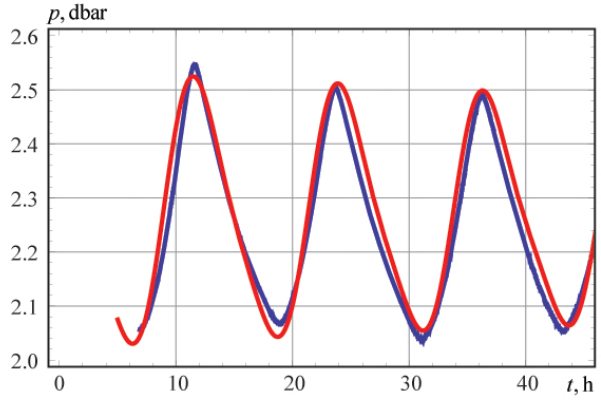

Fig. 9. Variations in the bottom pressure in the lake close to the channel (blue line), the measurements were made in 26–28 August 2009, at point 6; a fit with three sinusoids, relation (2) (red line).

important is the M_4 harmonic (period 6.21 h). The phase difference between M_2 and M_4 constituents of the tide causes asymmetry of the tide with uneven periods of flood and ebb. Asymmetry between crests and troughs of the record is caused by the phase difference between M_2 and M_4 harmonics initially induced by the tide choking over the bar.

We tried to find a simple fit of the tide amplitude variation using three sinusoidal tidal harmonics: M_2 (12.42 h), S_2 (12.00 h), and M_4 (6.21 h). The curve that fits the measured amplitude variation is shown in Fig. 9 with a red line. The fit was found using several iterations. First, we selected the amplitude of the M_4 harmonic by sorting different amplitudes with a step of 0.05 of the M_2 harmonic. The selection was made by finding the minimum root-mean-square deviation between the fit and measured bottom pressure variation. Then, we selected a fit by changing the phase of the M_4 harmonic with a step of 5°. A similar procedure was applied to the S_2 harmonic that changes the amplitude of the signal due to the spring–neap variability. Finally, we obtained the following fit:

$$h = h_0 + A_{M2}\cos(\omega_{M2}t) + 0.15A_{M2}\cos(\omega_{M4}t + 100^\circ) + 0.25A_{M2}\cos(\omega_{S2}t + 90^\circ), h_0 = 2.27\,\text{m}, A_M2 = 0.24\,\text{m}. \quad (2)$$

We note that no bottom friction and no bottom topography were introduced into the fit. They are included indirectly by the existence of the M_4 constituent. A surprising thing is that the point at which the flood dominant tide was recorded exists in the channel at a distance of only 50 m from the beginning of the channel.

5 Results of numerical simulations

The tidal asymmetry problem was raised in several publications (Huang et al., 2008; Cheng et al., 2010; Dias and Sousa, 2009) in which the authors investigated tidal asymmetry in narrow inlets. The model for calculations that we used in this study is described in the Appendix. Equation (A10), describing variations of the water surface elevation in the lake, is similar to Eq. (4) in the model of Stigebrandt (1980) describing the tidal choking effect in fjords. It was mentioned that the dependence of coefficient of resistance on the Reynolds number, bottom roughness and the form of the channel is most important for the simulations. In our case, the resistance is characterized by product κC, where C is the drag coefficient and κ characterizes the influence of variations of hydraulic radius and water speed over the channel on the

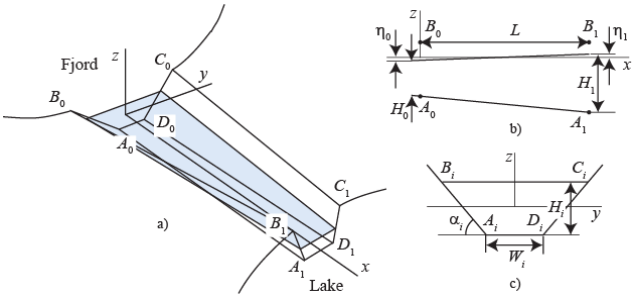

Fig. 10. Scheme of the channel: 3-D **(a)** and projections **(b, c)**.

resistance. We use average characteristics of the channel and assume that $\kappa = 1$. Thus, we obtain that drag coefficient C is the most important for the numerical simulations. The value of coefficient $C = 0.01$ was chosen based on the paper of Mofield (1988) when representative water depth is 1 m and seabed roughness is slightly above 1 cm.

Numerical modeling was performed for a channel of trapezoidal shape shown in Fig. 10a. The length of the channel in the x direction is L, the bottom of the channel is slightly inclined, and the water level elevation changes along the channel (Fig. 10b). Vertical cross sections of the channel at the fjord side and at the lake side have a trapezoidal shape: $A_0B_0C_0D_0$ and $A_1B_1C_1D_1$ in Fig. 10c. The bases of the trapezoids are equal to W_0 and W_1, and slope angles of their lateral sides are equal to α_0 and α_1. The thicknesses of the water levels above the bases are equal to H_0 at the fjord side and H_1 at the lake side, and the depths of undisturbed water in the channel are equal to $h_0 = H_0 - \eta_0$ and $h_1 = H_1 - \eta_1$, respectively.

The squares of areas A_i and hydraulic radii R_i are calculated using the following equations:

$$A_i = \frac{H_i^2}{\tan\alpha_i} + H_i W_i, \quad R_i = \frac{A_i}{P_i},$$
$$P_i = \frac{2H_i}{\sin\alpha_i} + W_i, \quad i = 0, 1. \tag{3}$$

Numerical simulations were performed with the following numerical values, which are close to those in the natural conditions:

$$S_l = 537\,800\ \mathrm{m}^2, \quad L = 100\ \mathrm{m}, \quad W_0 = 7\ \mathrm{m}, \quad W_1 = 3\ \mathrm{m},$$
$$\alpha_{0,1} = 30^\circ, \quad h_0 = 1.2\ \mathrm{m}, \quad h_1 = 1.5\ \mathrm{m},$$
$$C = 0.01, \quad \kappa = 1. \tag{4}$$

S_l is the square of the lake. The values in Eq. (4) correspond to geometrical characteristics of the channel. The drag coefficient corresponds to very shallow water conditions and high water velocities, therefore it is relatively high.

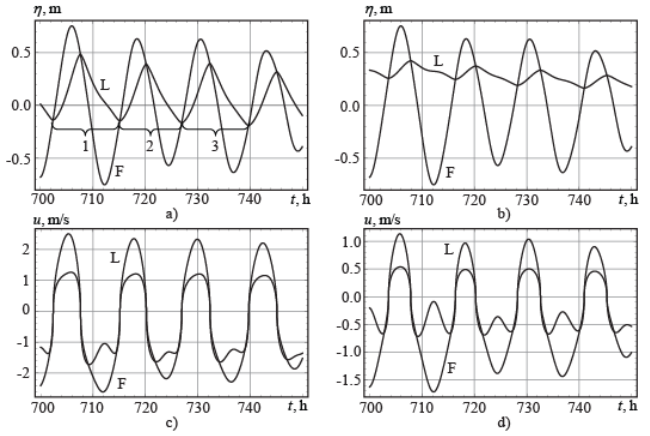

Fig. 11. Model calculations of water level that demonstrate tidal asymmetry. Variations in the water level at the lake side (L) and at the fjord side (F) at low tide **(a)** and high tide **(b)**. Variations in the water velocity at L and at F at low tide **(c)** and high tide **(d)**. Braces in Fig. 11a show the time intervals used for comparison in Fig. 12b.

Water level variations at the fjord side of the channel (forcing) are determined by function

$$\eta_0 = A_{M2}\cos(\omega_{M2}t + (v_0+u)_{M2} - G_{M2}) + A_{S2}\cos(\omega_{S2}t + (v_0+u)_{S2} - G_{S2}) + A_{K1}\cos(\omega_{K1}t + (v_0+u)_{K1} - G_{K1}) + A_{K2}\cos(\omega_{K2}t + (v_0+u)_{K2} - G_{K2}) + A_{N2}\cos(\omega_{N2}t + (v_0+u)_{N2} - G_{N2}), \tag{5}$$

where numerical values of harmonic constants A, ω and G are given in Table 1; the values of initial arguments $(v_0+u)_i$ are calculated using standard astronomical tables, and values of reduction coefficients are assumed equal to 1 (Vladimirsky, 1941).

The results of the numerical simulations are illustrated in Fig. 11. Figure 11a shows that the simulated variations in the water level at the lake side are very similar to the measured values shown in Fig. 4. Simulated water velocities at the fjord side shown in Fig. 11c are very similar to the velocities measured using the Aquadopp current meter (Fig. 6). The maximum velocities are reached at the lake side of the channel when the water level in the fjord is close to the maximum and at the fjord side of the channel when the water level in the fjord is close to the minimum. Their maximum absolute values exceed $2\,\mathrm{m\,s^{-1}}$. Model calculations demonstrate that the tidal flow in the channel is flood dominant.

Figure 11b shows that a constriction of the channel due to the ice formation in the wintertime explains the decrease in the tidal amplitude and the duration of the flood phase of the tide in the lake measured in the ice season (Fig. 7). Figure 11d demonstrates the decrease of the current velocities in the channel due to constriction.

Table 4. Absolute values of the amplitude ratios of M_2 and M_4 tides in the lake.

Ratio of amplitudes	Measurements related to intervals 1 and 2 shown in Fig. 4c		Three consecutive intervals of model calculation. The graphs are shown in Fig. 11b		
	1	2	1	2	3
$\lvert a_4/a_2\rvert$	0.196	0.198	0.232	0.178	0.177

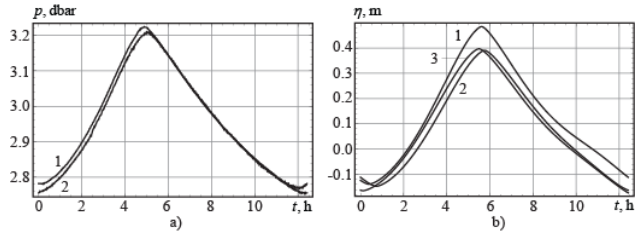

Fig. 12. Water pressure at the bottom of the lake measured in two consecutive periods of semidiurnal tide versus time **(a)** (see Fig. 4c). Water level in the lake calculated in three consecutive periods of semidiurnal tide versus time **(b)**.

Figure 12a shows water pressure variation at the bottom of the lake measured during two consecutive periods of semidiurnal tide (12.42 h) versus time (see Fig. 4c), and Fig. 12b shows an example of water level variations in the lake calculated in three consecutive periods of semidiurnal tide.

These graphs were used for the analysis of the change in the form of tide elevation. Curves 1 and 2 in Fig. 12a correspond to intervals 1 and 2 in Fig. 4c. Curves 1, 2 and 3 in Fig. 12b correspond to intervals 1, 2 and 3 in Fig. 11a. Each of the curves shown in Fig. 12 was approximated by the equation

$$F = a_1 + a_2\cos(\omega_{M2}t + a_3) + a_4\cos(2\omega_{M2}t + a_5). \quad (6)$$

Constants a_i were calculated using operations FindFit in "Mathematica 8". The absolute values of the calculated ratios $|a_4/a_2|$ of M_2 and M_4 tide amplitudes in the lake are shown in Table 4. The ratios $|a_4/a_2|$ calculated with field data are close to the ratios calculated for simulated tides in the lake.

6 Discussion

The physical interpretation of the change in the form of the tide is explained by the presence of a shallow rocky bar where the channel connects with the fjord. The depth of this bar in the low water phase is less than 1 m. This is the tidal choking effect considered in Stigebrandt (1980) and McClimans (1977). The presence of the bar leads to the generation of the second harmonic of semidiurnal tide; hence the form of the tide elevation changes. Different harmonics of the tide lose different parts of their energy when passing over a sill before flowing into the channel. Ice conditions in winter enhance this effect.

We attribute this rapid change in the asymmetric form of the tide to a very small scale of the experiment. Usually, such transition occurs over distances of the order of 1 km (Dronkers, 1986; Nidzieko, 2010). The horizontal scales of the channel are of the order of a few kilometers and the depth scale is of the order of a few tens of meters. In our case, the Littrowneset Channel is only 10 m wide and 1–2 m deep, which is two orders of magnitude smaller than the usual scales in straits and estuaries where tidal asymmetry was observed (Friedrichs and Aubrey, 1994; Blanton et al., 2002; Lanzoni and Seminara, 1998; Savenije and Veling, 2005). We can suppose that such change in the scales can lead to a decrease in the horizontal scale over which tidal asymmetry forms.

7 Conclusions

The tide in shallow places becomes asymmetric due to nonlinear effects caused by the influence of the bottom and especially by choking of the tidal flow over a sill that is located between the fjord and channel.

The form of asymmetric tide in the channel can be satisfactory approximated using the M_2 harmonic and only two additional tidal components: S_2 and M_4.

Measurements in the channel (Littrowneset) demonstrate that strong asymmetric effects develop over a distance of 50 m, very close to the sill that chokes the tidal flow.

The causes of such rapid development can be related to the small scale of the channel, which is two orders of magnitude smaller than the coastal channels connecting the open sea and lagoons, and in the estuaries, where tidal asymmetry is usually observed.

Appendix A

A model of tide in the lake

We suggest a model based on the measurements in the channel connecting Lake Vallunden with the fjord. The measurements are illustrated in Figs. 10 and 11. The objective of the model is to find relations between amplitudes of tidal elevations in the fjord and in the lake.

A model of water level variations in the lake is based on the equation of mass balance:

$$\frac{\mathrm{d}V_\mathrm{l}}{\mathrm{d}t} = A_1 u_1, \tag{A1}$$

where V_l is the water volume in the lake, A_1 is the area of the vertical cross section of the channel at the entrance to the lake, and u_1 is the water speed averaged over area A_1.

The current in the channel is described by the equations of mass and momentum balance:

$$\frac{\partial A}{\partial t} + \frac{\partial (Au)}{\partial x} = 0, \tag{A2}$$

$$\frac{\partial u}{\partial t} + u\frac{\partial u}{\partial x} = -g\frac{\partial \eta}{\partial x} - CR^{-1}|u|u, \tag{A3}$$

where t is time, x is the spatial coordinate directed along the channel from the fjord to the lake, A is the area of the vertical cross section of the channel, u is the water speed averaged over area A, η is the elevation of the water surface, R is the hydraulic radius of the channel, and C is the drag coefficient. The hydraulic radius is calculated using the equation $R = A/P$, where P is the wetted perimeter of the channel.

Terms $\partial A/\partial t$ and $\partial u/\partial t$ can be ignored in Eqs. (A2) and (A3) since a representative timescale of the problem is about one half of the semidiurnal period, i.e., 6 h. It is assumed that temporal variations of the current speed along the channel are determined by the variations in the water level gradient ($\partial\eta/\partial x$) along the channel, and the direction of the water velocity in the channel is opposite to the water level gradient over the channel:

$$u = -|u|\,\mathrm{sign}(\eta_1 - \eta_0). \tag{A4}$$

We integrate Eqs. (A2) and (A3) over the channel length taking into account (Eq. A4) and get

$$A_1 u_1 = A_0 u_0, \tag{A5}$$

$$\frac{u_1^2 - u_0^2}{2} + g(\eta_1 - \eta_0) = C\int_0^L R^{-1}u^2\mathrm{d}x\ \mathrm{sign}(\eta_1 - \eta_0), \tag{A6}$$

where A_0 and u_0 are the area of vertical cross-section of the channel at the entrance to the fjord and the water speed averaged over area A_0, respectively; η_0 and η_1 are the elevations of the water surface at the fjord side of the channel and at the lake side of the channel, respectively.

The integral in the right part of Eq. (A6) is approximated by the equation

$$\int_0^L R^{-1}u^2\mathrm{d}x = \kappa\langle R\rangle^{-1}\langle u\rangle^2 L, \tag{A7}$$

where $\langle R\rangle$ and $\langle u\rangle$ are mean values of the hydraulic radius and water velocity over the channel, respectively, and κ is the empirical coefficient characterizing changes of the hydraulic radius and water speed over the channel.

The mean values of the hydraulic radius and the water speed are approximated by the following equations:

$$\langle R\rangle = \frac{R_0 + R_1}{2}, \quad \langle u\rangle = \frac{u_0 + u_1}{2}, \tag{A8}$$

where R_0 and R_1 are the hydraulic radii at the fjord side of the channel and at the lake side of the channel.

We substitute Eqs. (A7) and (A8) in Eqs. (A5) and (A6), exclude u_0 and get

$$u_1 = -\mathrm{sign}(\eta_1 - \eta_0)\sqrt{\frac{2g(\eta_1 - \eta_0)}{A_1^2A_0^{-2} + 0.5\kappa C\langle R\rangle^{-1}L(A_1A_0^{-1}+1)^2 - 1}}. \tag{A9}$$

We assume that the variations in the water volume in the lake are expressed by the equation $\mathrm{d}V_\mathrm{l} = S_\mathrm{l}d\eta_1$ and substitute Eq. (A9) in Eq. (A1). We find that the equation describing water level variation in the lake caused by tidal variations of water level in the fjord is written as

$$S_\mathrm{l}\frac{\mathrm{d}\eta_1}{\mathrm{d}t} = -\mathrm{sign}(\eta_1 - \eta_0)A_1\sqrt{\frac{2g(\eta_1 - \eta_0)}{A_1^2A_0^{-2} + 0.5\kappa C\langle R\rangle^{-1}L(A_1A_0^{-1}+1)^2 - 1}}. \tag{A10}$$

Areas A_0 and A_1 are functions of the channel's bottom shape and the water surface elevations η_0 and η_1. Tidal variations of the water level in the fjord are determined by function $\eta_0(t)$.

Acknowledgements. This research was supported by the Norwegian Research Council (NFR) (project no. 196138/S30) and by the Russian Foundation for Basic Research (projects 11-08-00076, 11-05-00448, 10-08-01010, and 09-05-00599. We thank Z. Kowalik for the valuable comments to the paper, S. Muzylev and V. Gorbatsky for their assistance in field works and N. Marchenko for geographical mapping.

Edited by: H. Kalisch
Reviewed by: J. Berntsen and two anonymous referees

References

Aubrey, D. G. and Speer, P. E.: A study of non-linear tidal propagation in shallow inlet/estuarine systems, Part I: Observations, Estuarine, Coast. Shelf Sci., 21, 185–205, 1985.

Boon, J. D. and Byrne, R. J.: On basin hypsometry and the morphodynamic response of coastal inlets, Marine Geol., 40, 27–48, 1981.

Blanton, J. O., Lin, G. Q., and Elston, S. A.: Tidal current asymmetry in shallow estuaries and tidal creeks, Cont. Shelf Res., 22, 1731–1743, 2002.

Caline, F.: Coastal sea ice conditions around a breakwater in a microtidal, inner-fjord river delta in Svalbard, Ph. D. thesis, University Center in Svalbard, 2009.

Cheng, P., Valle-Levinson, A., and de Swart, H. E.: Residual currents induced by asymmetric tidal mixing in weakly stratified narrow estuaries, J. Phys. Oceanogr., 40, 2135–2147, 2010.

Dias, J. M. and Sousa, M. C.: Numerical modeling of Ria Formosa tidal dynamics, J. Coast. Res., 56, 1345–1349, 2009.

Dronkers, J.: Tidal asymmetry and estuarine morphology, Netherlands, J. Sea Res., 20, 117–131, 1986.

Farmer, D. M. and Freeland, H. J.: The physical oceanography of fjords, Prog. Oceanogr., 12, 147–219, 1983.

Fer, I. and Widell, K.: Early spring turbulent mixing in an ice-covered Arctic fjord during transition to melting, Cont. Shelf Res., 27, 1980–1999, 2007.

Friedrichs, C. T. and Aubrey, D. G.: Tidal propagation in strongly convergent channels, J. Geophys. Res., 99, 3321–3336, 1994.

Gallagher, B.: Model for nonlinear tides in small basins with openings of restricted depth, J. Geophys. Res., 78, 6395–6400, 1973.

Hoitink, A. J. F., Hoekstra, P., and van Maren, D. S.: Flow asymmetry associated with astronomical tides: Implications for the residual transport of sediment, J. Geophys. Res., 108, 3315–3323, doi:10.1029/2002JC001539, 2003.

Huang, H., Chen, C., Blanton, J. O., and Andrade, F. A.: Estuarine, Coastal and Shelf Science: A numerical study of tidal asymmetry in Okatee Creek, South Carolina, 78, 190–202, 2008.

Lanzoni, S. and Seminara, G.: On tide propagation in convergent estuaries, J. Geophys. Res., 103, 30793–30812, 1998.

McClimans, T. A.: On the energetics of tidal inlets to land-locked fjords, Marine Sci. Comm., 4, 121–137, 1977.

Mirfendersk, H. and Tomlinson, R.: Living with sea-level rise and climate change: observation and analysis of hydrodynamic parameters in tidal inlets in a predominantly semidiurnal regime, J. Coast. Res., 24, 1229–1239, 2008.

Mofjeld, H. O.: Depth dependence of bottom stress and quadratic drag coefficient for barotropic pressure-driven currents, J. Phys. Oceanogr., 18, 1658–1669, 1988.

Nidzieko, N. J.: Tidal asymmetry in estuaries with mixed semidiurnal/diurnal tides, J. Geophys. Res., 115, C08006, doi:10.1029/2009JC005864, 2010.

Savenije, H. H. G. and Veling, E. J. M.: Relation between tidal damping and wave celerity in estuaries, J. Geophys. Res., 110, C04007, doi:10.1029/2004JC002278, 2005.

Stigebrandt, A.: Some aspects of tidal interactions with fjord constrictions, Estuar. Coast. Mar. Sci., 2, 151–166, 1980.

Støylen, E. and Weber, E.: Mass transport induced by internal Kelvin waves beneath shore-fast ice, J. Geophys. Res., 115, C03022, doi:1029/2009JC005298, 2010.

Vladimirsky, N. P. (Ed.): Rukovodstvo po obrabotke I predskazaniu prilivov (1941), Gidrograficheskoe upravlenie VMF USSR, Leningrad, 347 pp., (Handbook for the Processing and Prediction of Tides), 2010.

Walton Jr., T. L.: Tidal velocity asymmetry at inlets, ERDC/CHL CHETN IV-47, US Army Engineer Research and Development Center, Vicksburg, MS, available at: http://chl.erdc.usace.army.mil, last access: 27 September 2013, 2002.

Wrangborg, D., Grady, R., Marchenko, A., and Karulin, E.: Analysis of Tidal Deformations of Land Fast Ice in Shallow Arctic Fjord, Proceedings of the 22 International Conference on Port and Ocean Engineering under Arctic Conditions 9–13 June 2013, Espoo, Finland, 2013.